Conditions for observing Shapiro steps in a $Bi_2Sr_2CaCu_2O_{8+\delta}$ high-T_c superconductor intrinsic Josephson junction: Numerical calculations

Michihide Kitamura, Akinobu Irie, and Gin-ichiro Oya
Department of Electrical and Electronic Engineering, Utsunomiya University, 7-1-2 Yoto, Utsunomiya, Tochigi 321-8585, Japan
(Received 3 October 2006; revised manuscript received 6 February 2007; published 14 August 2007)

Conditions to observe Shapiro steps clearly and stably are studied for an intrinsic Josephson junction (IJJ) in $Bi_2Sr_2CaCu_2O_{8+\delta}$ high-T_c superconductors. The current equation normalized by the critical current $I_c(T)$ is solved fully numerically. In the calculations, the quasiparticle tunneling current is evaluated by using the normalized *I-V* characteristics obtained within the *d*-wave symmetry superconducting gap, while the Cooper-pair (CP) one is calculated on the basis of the general way in which the coherent and incoherent CP tunneling currents can be correctly calculated within the *d*-wave treatment and the current due to thermal noises is also simulated by using normal random numbers. It is found that the product SR_{shunt} of the junction cross section S and the shunt resistance R_{shunt}, and the critical current density J_c are important junction parameters, and moreover, that the current equation of the IJJ with no shunt resistance depends on only a universal curve $\mu(i_0)$ as a function of the normalized external dc current i_0. Furthermore, the effects of the noise, the normalized CP tunneling currents, the SR_{shunt} product, the normalized amplitude i_r of external ac modulation, and the J_c on observing the Shapiro steps are studied. When the IJJ is operated under the condition that the shunt resistance is added and the external ac modulation frequency f_r is higher than the plasma frequency f_p, it is found that (1) clear and stable Shapiro steps with good responses are obtained within the wide range of i_r, (2) the response does not so largely depend on the value of SR_{shunt}, and (3) the response for the high J_c junction is much better than that for the low one.

DOI: 10.1103/PhysRevB.76.064518 PACS number(s): 74.72.Hs, 74.50.+r, 74.40.+k

I. INTRODUCTION

In 1963, Shapiro did an experiment on the effect of microwave irradiation on the dc current *I*-voltage *V* characteristics of a Josephson junction $Al/Al_2O_3/Sn$ and showed that when the microwave is applied to the Josephson junction, clear current steps are observed on the quasiparticle (QP) branches of the dc *I-V* characteristics and those steps, which are now called "Shapiro steps," are observed on constant voltages given by $n\Phi_0 f_r$ $(n=\pm 1, \pm 2, \ldots)$.[1] Here the Φ_0 is a flux quantum $(=2.067\,85\times 10^{-15}$ Wb) defined by $h/2e$ using Planck constant h so that this is a universal constant. The f_r is the frequency of the applied microwave and the value of f_r can be very well identified so that a voltage $\Phi_0 f_r$ can be used as a quantum voltage standard. The Shapiro steps are one of the important phenomena observed from a Josephson junction.

It is well known that the high-T_c cuprate superconductors, such as $YBa_2Cu_3O_{6+\delta}$ (YBCO), $Bi_2Sr_2CaCu_2O_{8+\delta}$ (BSCCO), $(Pb_yBi_{1-y})_2Sr_2CaCu_2O_{8+\delta}$ (PBSCCO), and $Tl_2Ba_2Ca_2Cu_3O_{10+\delta}$ (TBCCO), are strongly anisotropic and show the intrinsic Josephson effect so that these crystals can be regarded as a stack of atomic-scale Josephson junctions called intrinsic Josephson junctions (IJJ's).[2–8] From the direct measurements of all dc and ac Josephson effects with current flow in the *c*-axis direction, Kleiner and Müller pointed out that the IJJ's in the high-T_c cuprate superconductors are superconductor-insulator-superconductor (SIS)-type Josephson junctions.[3] According to these experimental results, the Shapiro steps can also be observed on the IJJ's in the high-T_c cuprate superconductors, which are characterized by the *d*-wave symmetry superconducting gap rather than the *s* one.[9–11] Actually, many experiments on the Shapiro steps have been done for the BSCCO single crystals.[12–18]

A qualitative understanding about the Shapiro steps is obtained by using a simple model based on a "voltage biased" configuration. However, the experiments of the *I-V* characteristics are done within a framework of a "current source" configuration. Therefore, the current source model must be used to understand the nature of Shapiro steps. The starting point of the current source model is a current conservation such as

$$I_{cap}(t) + I_{shunt}(t) + I_{QP}(t,T) + I_{CP}(t,T) = I_{ext}(t,T), \qquad (1)$$

where t is the real time and T is the sample temperature. The $I_{ext}(t,T)$ is the current supplied from the external current source. The $I_{cap}(t)$ is the current flowing through the capacitance C, which is given by $(C\hbar/2e)d^2\varphi(t)/dt^2$, and the $I_{shunt}(t)$ is that through the *externally* added shunt resistance R_{shunt}, given by $(1/R_{shunt})(\hbar/2e)d\varphi(t)/dt$. The $\varphi(t)$ is the phase difference between order parameters of two superconductors, which make the SIS Josephson junction. The $I_{QP}(t,T)$ is the current due to the quasiparticle (QP) tunneling. For the QP tunneling current, we have already proposed a model based on the *d*-wave symmetry superconducting gap and calculated the normalized QP tunneling *I-V* characteristics and showed that the overall profile of the experimental *I-V* characteristics is very well explained by our model calculations.[19] In the present paper, therefore, we evaluate the QP current $I_{QP}(t,T)$ as

$$I_{QP}(t,T) = \frac{\hbar}{2eR_{QP}(I_{dc},T)}\frac{d\varphi(t)}{dt}, \qquad (2)$$

where $R_{QP}(I_{dc},T)$ is the resistance due to the QP tunneling and is evaluated by using the normalized dc *I-V* characteris-

tics we have already calculated. In our calculations for the normalized dc *I-V* characteristics, we focused our attention to the overall profile of the *I-V* characteristics.[19] The $I_{CP}(t,T)$ in Eq. (1) is the current due to the Cooper pair (CP) tunneling and is usually evaluated as $I_c(T)\sin\varphi(t)$ using the critical current $I_c(T)$ and the phase difference $\varphi(t)$. In addition to this simple expression for the $I_{CP}(t,T)$, in the present paper, we present a general expression for the $I_{CP}(t,T)$ within a framework of the *d*-wave symmetry superconducting gap and calculate the normalized current $i_{CP}(t,T)$ defined by $I_{CP}(t,T)/I_c(T)$.

On the BSCCO at 4.2 K, it is experimentally known that when the cross section S of the junction is larger than 1 μm^2, the jump voltage V_{jump}, which is a voltage appearing when the external current is just equal to $I_c(T)$, is independent of S and is $26\sim31$ mV,[20] which is much smaller than the gap voltage V_g of ~50 mV owing to the $I_c(T)$ much smaller than that defined by $\pi\Delta(0)/2eR_{QP}(I_{dc},T)$, where $\Delta(0)$ is the superconducting energy gap at 0 K. Namely, for the BSCCO at 4.2 K, the V_{jump} can be regarded as a universal constant whose value has been selected as 28 mV from an averaging. Moreover, it is also experimentally known that when the S is larger than 1 μm^2, the critical current density J_c does not so strongly depend on S and locates 700–1500 A/cm^2 at 4.2 K.[20] In the present paper, we consider the case that the sample temperature T is 4.2 K and the cross section S of the junction is larger than 1 μm^2, so that the critical current density J_c could also be regarded as a universal constant for BSCCO at 4.2 K. In the following, the J_c is set to 1000 A/cm^2 at 4.2 K for simplicity.

Using the resistively shunted junction (RSJ) model, in which the effective resistance $R_{QP}^{(eff)}(I_{dc})$ of a junction due to the QP tunneling is set to an appropriate constant value R_{app} (usually set to a normal resistance R_N), Kautz and Monaco extensively studied the nature of Shapiro steps on the SIS Josephson junction.[21] They found that when $\beta_c>1$ there is a chaotic region defined by $\beta_c^{-1}\leqslant\Omega\leqslant\beta_c^{-1/2}$ in which Shapiro steps cannot be observed. The Ω is the normalized frequency defined by ω_r/ω_m and β_c is the McCumber parameter defined by $R^*C\omega_m$, where $\omega_m\equiv 2eI_cR^*/\hbar$ and $1/R^*=1/R_{app}+1/R_{shunt}$. Therefore, the chaotic region can be rewritten as

$$\frac{1}{2\pi R^*C}(\equiv f_{RC})\leqslant f_r\leqslant f_p, \tag{3}$$

where $2\pi f_r=\omega_r$ and the plasma frequency f_p is calculated as $2\pi f_p=\sqrt{2eI_c/\hbar C}$. The critical current I_c is equal to J_cS and the capacitance C is easily calculated as $\varepsilon\varepsilon_0 S/d$ by using $d=12$ Å and dielectric constant $\varepsilon=7$.[8]

Therefore, the plasma frequency f_p of an IJJ in BSCCO at 4.2 K can be regarded as a universal constant calculated as 122 GHz. On the BSCCO at 6 K, Wang *et al.* observed clear Shapiro steps when $f_r=1.6$ and 2.5 THz (Ref. 13) and 760 GHz.[15] This is reasonable, because the f_p at 6 K is nearly equal to 122 GHz as $I_c(6)\simeq I_c(4.2)$ so that the microwave frequency f_r is much larger than $f_p=122$ GHz; that is, $f_r\gg f_p$.

It is very useful to fabricate a Shapiro step device by using the intrinsic Josephson junctions (IJJs) in BSCCO. From this point of view, the aim of this paper is to present a theoretical guideline for observing the Shapiro steps on an IJJ in BSCCO with regard to its noise, i_0, i_r, SR_{shunt}, and J_c.

II. THEORY

The CP tunneling current $I_{CP}(t,T)$ in Eq. (1) can be generally written as[22]

$$I_{CP}(t,T)=\int_0^\infty \mathrm{Re}\{R'(t',T)\}\sin\frac{\varphi(t-t')+\varphi(t)}{2}dt', \tag{4}$$

and the $R'(t,T)$ is given by

$$R'(t,T)=-i\frac{\Theta(t)}{R_N}\frac{\hbar}{\pi e}\int_{-\infty}^{\infty}d\omega\int_{-\infty}^{\infty}d\omega' e^{-i(\omega-\omega')t}p_L(\omega)p_R(\omega') \times\{f(\omega')-f(\omega)\}, \tag{5}$$

where $\Theta(t)$ is a step function such as 1 for $t\geqslant 0$ and 0 for $t<0$ and $f(\omega)$ is the Fermi-Dirac distribution function. By setting $t-t'$ to t'', the $I_{CP}(t,T)$ is represented as

$$I_{CP}(t,T)=\frac{\hbar}{\pi eR_N}\times\int_{-\infty}^{t}dt''\left[\sin\frac{\varphi(t'')+\varphi(t)}{2}\times\int_{-\infty}^{\infty}d\omega\int_{-\infty}^{\infty}d\omega'\,\sin(\omega-\omega')(t-t'')\times p_L(\omega)p_R(\omega')\{f(\omega)-f(\omega')\}\right]. \tag{6}$$

Here note that the $p_j(\omega)$ is the pair density of states of superconductor $j(=L,R)$ and is represented as

$$p_j(\omega)=\frac{|\Delta_j|}{\sqrt{\omega^2-\Delta_j^2}}\,\mathrm{sgn}(\omega)\Theta(|\omega|-|\Delta_j|), \tag{7}$$

where Δ_j is the superconducting energy gap of superconductor j and $\mathrm{sgn}(\omega)$ is a sign function such as 1 for $\omega\geqslant 0$ and -1 for $\omega<0$. The critical current $I_c(T)$ as a function of temperature T is given by

$$I_c(T)=\frac{\hbar}{\pi eR_N}P\int_{-\infty}^{\infty}d\omega\int_{-\infty}^{\infty}d\omega'\frac{f(\omega)-f(\omega')}{\omega-\omega'}p_L(\omega)p_R(\omega'). \tag{8}$$

Therefore, the normalized CP tunneling current $i_{CP}(t,T)$ defined by $I_{CP}(t,T)/I_c(T)$ is given by

$$i_{CP}(t,T)=\int_{-\infty}^{t}h_{CP}(t,t',T)dt'. \tag{9}$$

Here the $h_{CP}(t,t',T)$ is the kernel for the CP tunneling current and is represented as

$$h_{CP}(t,t',T) = \sin\frac{\varphi(t')+\varphi(t)}{2} \times \frac{\int_{-\infty}^{\infty} d\omega \int_{-\infty}^{\infty} d\omega' \sin(\omega-\omega')(t-t')p_L(\omega)p_R(\omega')\{f(\omega)-f(\omega')\}}{P\int_{-\infty}^{\infty} d\omega \int_{-\infty}^{\infty} d\omega' \frac{f(\omega)-f(\omega')}{\omega-\omega'} p_L(\omega)p_R(\omega')} \equiv \sin\frac{\varphi(t')+\varphi(t)}{2} w_{CP}(t,t',T). \tag{10}$$

By using two relations $f(-\omega)=1-f(\omega)$ and $p(-\omega)=-p(\omega)$, and by changing the variable such as $\omega \to E(=\hbar\omega)$, the $w_{CP}(t,t',T)$ defined in Eq. (10) can be rewritten as

$$\hbar w_{CP}(t,t',T) = \frac{\int_0^{\infty} dE \int_0^{\infty} dE' p_L(E)p_R(E') \left[\{f(E)-f(E')\}\sin\frac{E-E'}{\hbar}(t-t') + \{1-f(E)-f(E')\}\sin\frac{E+E'}{\hbar}(t-t') \right]}{P\int_0^{\infty} dE \int_0^{\infty} dE' p_L(E)p_R(E') \left[\frac{f(E)-f(E')}{E-E'} + \frac{1-f(E)-f(E')}{E+E'} \right]}$$

$$\equiv \kappa_{CP}(t-t',T). \tag{11}$$

In general, the quasiparticle excitation energy E is a function of the wave-number vector $\mathbf{k}$ characterizing a Cooper pair. In the case of d-wave symmetry superconductors, this is true since the superconducting gap of the d-wave symmetry superconductor shows an explicit $\mathbf{k}$-vector dependence. Therefore, Eq. (11) must be translated into a form in which the wave-number vector $\mathbf{k}$ is regarded as the basic variable instead of E. We will show its explicit form later.

As can be seen from Eq. (11), in the following consideration only the E with a positive value is taken into account. Therefore, the $p_j(E)$ defined by Eq. (7) can be rewritten as

$$p_j(E) = \frac{|\Delta_j|}{\sqrt{E^2-\Delta_j^2}}\Theta(E-|\Delta_j|) = \frac{E}{\sqrt{E^2-\Delta_j^2}}\Theta(E-|\Delta_j|)\frac{|\Delta_j|}{E} = n_j(E)\frac{|\Delta_j|}{E}. \tag{12}$$

Here, $n_j(E)$ is the quasiparticle density of states, evaluated as

$$n_j(E) = \frac{1}{N_j(E_F)}\sum_{\mathbf{k}_j}^{BZ_1} \delta(E-E_{\mathbf{k}_j}), \tag{13}$$

where the BZ_1 means the first Brillouin zone and $N_j(E_F)$ is the one-electron density of states at the Fermi level of superconductor j. By using the above two relations, we can get a final explicit form of $i_{CP}(\tau,T)$ as follows:

$$i_{CP}(\tau,T) = \int_{-\infty}^{\tau} K_{CP}(\tau-\tau',T)\sin\frac{\varphi(\tau')+\varphi(\tau)}{2}d\tau', \tag{14}$$

$$K_{CP}(\tau-\tau',T) = \frac{2\pi}{\omega_r}w_{CP}(\tau,\tau',T) = \frac{2\pi}{\hbar\omega_r}\kappa_{CP}(\tau-\tau',T), \tag{15}$$

where τ is the dimensionless time defined by $2\pi\tau=\omega_r t$. Here it should be noticed that the kernel $K_{CP}(\tau-\tau',T)$ satisfies the following relation:

$$\int_{-\infty}^{\tau} K_{CP}(\tau-\tau',T)d\tau' = \int_0^{\infty} K_{CP}(u,T)du = 1. \tag{16}$$

This relation is understood as follows: If we consider the simplest case such that the $\varphi(\tau)$ is given by a time independent constant value φ_0, that is, the zero-voltage state, Eq. (14) becomes

$$i_{CP}(\tau,T) = \sin\varphi_0 \int_{-\infty}^{\tau} K_{CP}(\tau-\tau',T)d\tau'. \tag{17}$$

As is well known, the $i_{CP}(\tau,T)$ is equal to $\sin\varphi_0$ when the junction is in the zero-voltage state, therefore, the kernel $K_{CP}(\tau-\tau',T)$ must satisfy the relation (16). The kernel $K_{CP}(\tau-\tau',T)$ can be written as $\frac{2\pi}{\hbar\omega_r}\kappa_{CP}(\tau-\tau',T)$ as shown in Eq. (15) and the explicit form of the kernel $\kappa_{CP}(\tau-\tau',T)$ $[=\hbar w_{CP}(\tau,\tau',T)]$ is given as

$$\kappa_{CP}(\tau-\tau',T) = \frac{\sum_{\mathbf{k}}^{BZ_1}\sum_{\mathbf{k}'}^{BZ_1}|H'_{\mathbf{k},\mathbf{k}'}|^2\frac{|\Delta_{\mathbf{k}}\Delta_{\mathbf{k}'}|}{E_{\mathbf{k}}E_{\mathbf{k}'}}\left[\{f(E_{\mathbf{k}})-f(E_{\mathbf{k}'})\}\sin\left\{\frac{E_{\mathbf{k}}-E_{\mathbf{k}'}}{\hbar\omega_r}2\pi(\tau-\tau')\right\}+\{1-f(E_{\mathbf{k}})-f(E_{\mathbf{k}'})\}\sin\left\{\frac{E_{\mathbf{k}}+E_{\mathbf{k}'}}{\hbar\omega_r}2\pi(\tau-\tau')\right\}\right]}{\sum_{\mathbf{k}}^{BZ_1}\sum_{\mathbf{k}'}^{BZ_1}|H'_{\mathbf{k},\mathbf{k}'}|^2\frac{|\Delta_{\mathbf{k}}\Delta_{\mathbf{k}'}|}{E_{\mathbf{k}}E_{\mathbf{k}'}}\left[\frac{f(E_{\mathbf{k}})-f(E_{\mathbf{k}'})}{E_{\mathbf{k}}-E_{\mathbf{k}'}}+\frac{1-f(E_{\mathbf{k}})-f(E_{\mathbf{k}'})}{E_{\mathbf{k}}+E_{\mathbf{k}'}}\right]}. \quad (18)$$

Here, $H'_{\mathbf{k},\mathbf{k}'}$ is the matrix element due to $\mathbf{k}\rightarrow\mathbf{k}'$ tunneling. It should be noted that the $H'_{\mathbf{k},\mathbf{k}'}$ for the coherent tunneling is proportional to $\delta_{\mathbf{k},\mathbf{k}'}$ and that for the incoherent one is given by a constant irrespective of $\mathbf{k}$ and $\mathbf{k}'$. In the practical calculations of $\kappa_{CP}(\tau-\tau',T)$ defined by Eq. (18), therefore, $H'_{\mathbf{k},\mathbf{k}'}$ is set to $\delta_{\mathbf{k},\mathbf{k}'}$ for the coherent tunneling and to 1 for the incoherent one. The quasiparticle excitation energy $E_{\mathbf{k}}$ is given by $\sqrt{\xi_{\mathbf{k}}^2+\Delta_{\mathbf{k}}^2}$. The $\Delta_{\mathbf{k}}$ is the superconducting energy gap and it is well known that the $\Delta_{\mathbf{k}}$ of the *d*-wave symmetry superconductor is represented as $\Delta(T)\cos 2\phi_k$, where ϕ_k is the angle of the $\mathbf{k}$ vector measured from the *x* axis.[10] The $\xi_{\mathbf{k}}$ is the one-electron energy relative to the Fermi level. By doing the band structure calculation, we got the values of $\xi_{\mathbf{k}}$ as full numerical data.[19]

III. CALCULATION

The external current $I_{ext}(t,T)$ in Eq. (1) consists of a constant current I_0, a time dependent current $I_r \sin \omega_r t$ due to the external ac modulation with a frequency ω_r, and the current $I_{noise}(t,T)$ due to the noise at a finite temperature *T*. Namely, the $I_{ext}(t,T)$ is written as

$$I_{ext}(t,T) = I_0 + I_r \sin \omega_r t + I_{noise}(t,T). \quad (19)$$

We consider here a "white noise" as a noise so that the $I_{noise}(t,T)$ satisfies the following relations:

$$\langle I_{noise}(t,T)\rangle_t = 0,$$

$$\langle I_{noise}(t,T)I_{noise}(t+t',T)\rangle_t = \frac{2k_BT}{R_J}\delta(t'), \quad (20)$$

where $\langle A(t)\rangle_t$ means the time average of a time dependent function $A(t)$. The R_J is the resistance of a junction and is given by

$$\frac{1}{R_J} = \frac{1}{R_{QP}^{(eff)}(I_0)} + \frac{1}{R_{shunt}} \equiv \frac{1}{R_J(I_0)}, \quad (21)$$

because of $I_{dc}=\langle I_{ext}(t,T)\rangle_t = I_0$.

The white noises are made numerically by using random numbers. We write here the random numbers as $i_{random}^{(cal)}(t)$, which have been made by the normal random number generator (code name: NRAND) in the library program. The normalized white noise $i_{noise}(t,T)$ defined by $I_{noise}(t,T)/I_c(T)$ must be proportional to $i_{random}^{(cal)}(t)$; that is,

$$i_{noise}(t,T) = \eta(T) i_{random}^{(cal)}(t). \quad (22)$$

The autocorrelation $\langle i_{noise}(t,T)i_{noise}(t+t',T)\rangle_t$ is equal to $\eta(T)^2\langle i_{random}^{(cal)}(t)i_{random}^{(cal)}(t+t')\rangle_t$. Therefore, integrating the relation (20) over the t', we get

$$\frac{2k_BT}{I_c(T)^2R_J} = \eta(T)^2\int_{-\infty}^{\infty}\langle i_{random}^{(cal)}(t)i_{random}^{(cal)}(t+t')\rangle_t dt'. \quad (23)$$

Here, we define an absolute time resolution Δt. By doing some numerical calculations for the kernel, we found that Δt of 1×10^{-14} s (=10 fs) is small enough to resolve the structure of the kernel. The autocorrelation $\langle i_{random}^{(cal)}(t)i_{random}^{(cal)}(t+t')\rangle_t$ is also proportional to $\delta(t')$, so that the integral in Eq. (23) can be well evaluated as $\langle i_{random}^{(cal)}(t)^2\rangle_t\Delta t$. Therefore, the $\eta(T)$ is given by

$$\eta(T) = \sqrt{\frac{2k_BT}{\langle i_{random}^{(cal)}(t)^2\rangle_t\Delta t I_c(T)^2R_J}}, \quad (24)$$

so that from Eq. (22) we can get $i_{noise}(t,T)$ at *T* as full numerical data with a function of *t* defined by $n\Delta t$. All the experiments always include the effect of thermal noise. Therefore, all the calculations presented in the present paper also include the effect of the thermal noise, except for the special case we notice.

Now, we can easily get the real scaled dc *I-V* characteristics and the resultant resistance $R_{QP}(I_{dc})$ by using the normalized dc *I-V* characteristics calculated from our model based on the *d*-wave symmetry superconducting gap. According to the calculated results, the differential resistance $dV/dI[\equiv R_{dif}(I)]$ at $I=0$ is infinite. In other words, the theoretical calculation shows that the differential conductance $dI/dV[\equiv G(V)]$ at $V=0$ is zero. However, it was experimentally observed that the differential conductance $G(V)$ at $V=0$ on the *I-V* characteristics is not zero but finite.[13,23] The differential conductance $G(0)$ can be evaluated by using the experimental data. For example, Latyshev *et al.* pointed out that the $I(V)$ curve at low voltage region ($V<10$ mV) can be approximately represented as $aV+bV^3$ and estimated the values of adjustable parameters *a* and *b* by using their experimental $I(V)$ curves at low voltage region.[23] Their approximational treatment may be true since the $I(V)$ curve must be an odd function of *V*. The $G(0)$ is proportional to S/d, thus to J_cS $(=I_c)$. Therefore, the $G(0)[=1/R_{dif}(0)]$ is proportional to $I_c/V_{jump}\equiv 1/R_{jump}$ since the voltage V_{jump} is a universal con-

stant. Therefore, the differential resistance $R_{dif}(0)$ can be represented as γR_{jump} using a proportion constant γ. Wang *et al.* presented clear *I-V* characteristics for BSCCO.[13]

Their experiments show that the values of R_{jump} and $R_{dif}(0)$ are about 100 and 500 Ω, respectively, i.e., $\gamma \simeq 5$. In the following, therefore, the value of γ is set to 5. By using the $R_{dif}(0)$ and the $R_{QP}(I_{dc})$ evaluated from the real scaled dc *I-V* characteristics, the effective resistance $R_{QP}^{(eff)}(I_{dc})$ due to the QP tunneling is evaluated as a function of $I_{dc}(=I_0)$. In order to get the value of $R_{QP}^{(eff)}(I_0)$, we consider a parallel circuit consisting of $R_{QP}(I_{QP})$ and $R_{dif}(0)$. Here note that both the $R_{QP}(I_{QP})$ and $R_{dif}(0)$ are inversely proportional to S and that the $R_{dif}(0)$ is a constant but the $R_{QP}(I_{QP})$ is a function of current I_{QP}. The total current I_0 is equal to $I_{QP}+I_{dif}$, where the I_{QP} and I_{dif} are the currents passing through the resistances $R_{QP}(I_{QP})$ and $R_{dif}(0)$, respectively. Namely,

$$I_0 = I_{QP}\left(1 + \frac{R_{QP}(I_{QP})}{R_{dif}(0)}\right). \tag{25}$$

As already stated, by using the real scaled dc *I-V* characteristics, the value of $R_{QP}(I_{QP})$ can be obtained numerically as a function of I_{QP}, thus from Eq. (25) we can get a relation $I_0 = I_0(I_{QP})$ by a numerical form. It is easy to get an inverse relation $I_{QP}=I_{QP}(I_0)$ from the numerical relation $I_0=I_0(I_{QP})$. By using the relation $I_{QP}=I_{QP}(I_0)$ with a numerical form, therefore, the $R_{QP}^{(eff)}(I_0)$ in Eq. (21) as a function of I_0 is calculated as

$$\frac{1}{R_{QP}^{(eff)}(I_0)} = \frac{1}{R_{QP}(I_{QP}(I_0))} + \frac{1}{R_{dif}(0)} \propto S. \tag{26}$$

The current equation (1) normalized by the I_c is

$$\frac{1}{\omega_p^2}\frac{d^2\varphi(t)}{dt^2} + \frac{\hbar}{2eI_cR_J(I_0)}\frac{d\varphi(t)}{dt} + i_{CP}(t) = i_{ext}(t),$$

$$i_{ext}(t) = i_0 + i_r \sin \omega_r t + i_{noise}(t), \tag{27}$$

where $i_0 \equiv I_0/I_c$, $i_r \equiv I_r/I_c$, and $i_{noise}(t) \equiv I_{noise}(t)/I_c$. By using a dimensionless time τ defined by $2\pi\tau = \omega_r t$, Eq. (27) is rewritten as

$$\frac{d^2\varphi(\tau)}{d\tau^2} + 2\pi\left(\frac{f_p}{f_r}\right)\frac{\Phi_0 f_p}{I_cR_J(I_0)}\frac{d\varphi(\tau)}{d\tau} + (2\pi)^2\left(\frac{f_p}{f_r}\right)^2 \times\{i_{CP}(\tau) - i_{ext}(\tau)\} = 0, \tag{28}$$

where $2\pi f_p = \omega_p$ and $2\pi f_r = \omega_r$. It is sure that when the resistance $R_J(I_0)$ in Eq. (28) is set to a constant resistance R^* in Eq. (3) and the $i_{CP}(\tau)$ is evaluated as $\sin\varphi(\tau)$, Eq. (28) becomes the simplest resistively shunted junction (RSJ) current equation such that

$$\frac{d^2\varphi}{d\tau^2} + \frac{2\pi}{\beta_c\Omega}\frac{d\varphi}{d\tau} + \frac{(2\pi)^2}{\beta_c\Omega^2}(\sin\varphi - i_{ext}) = 0. \tag{29}$$

From Eqs. (28) and (29), it is seen that the dimensionless term $\Phi_0 f_p/I_cR_J(I_0)$ in Eq. (28) can be written as $1/\sqrt{\beta_c(I_0)}$ using the McCumber parameter $\beta_c(I_0)$ as a function of I_0. The plasma frequency f_p is now a universal constant with the value of 122 GHz for an intrinsic Josephson junction (IJJ) in BSCCO at 4.2 K, therefore, the voltage $\Phi_0 f_p$ is also a universal constant 252.4 μV. The dimensionless term $\Phi_0 f_p/I_cR_J(I_0)$ is the most important term to understand the nature of Shapiro steps observed on the BSCCO. From Eq. (21), the term $\Phi_0 f_p/I_cR_J(I_0)$ is written as

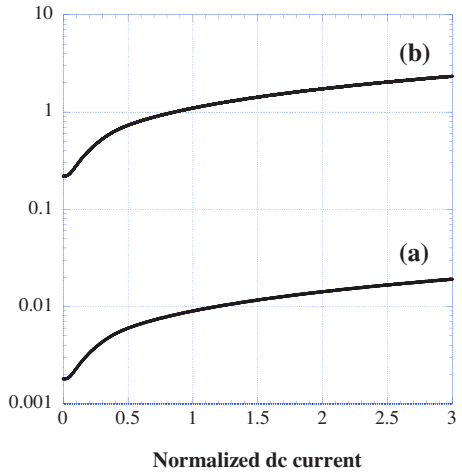

FIG. 1. (Color online) Universal curves (a) $\mu(i_0)$ in dimensionless and (b) $f_{RC}^{(NS)}(i_0)$ in GHz as a function of the normalized dc current $i_0(\equiv I_0/I_c)$, where I_0 is the external dc current and I_c is the critical current of the Josephson junction. The $\mu(i_0)$ is defined by the voltage ratio $\Phi_0 f_p/I_cR_{QP}^{(eff)}(I_0)$ and the $f_{RC}^{(NS)}(i_0)$ is the frequency defined by $1/2\pi R_{QP}^{(eff)}(I_0)C$, so that the ratio $f_{RC}^{(NS)}(i_0)/\mu(i_0)$ is equal to the plasma frequency f_p of a junction, which is a universal constant, where Φ_0 is a flux quantum, $R_{QP}^{(eff)}(I_0)$ is the resistance defined by Eq. (26), and C is the capacitance of a junction. It should be emphasized that two universal curves $\mu(i_0)$ and $f_{RC}^{(NS)}(i_0)$ are functions of not I_0 but i_0, so that these curves are always valid for all the intrinsic Josephson junctions in BSCCO including no shunt resistance. Note that the McCumber parameter $\beta_c^{(NS)}(i_0)$ for no shunt case is equal to a universal curve $1/\mu^2(i_0)$.

$$\frac{\Phi_0 f_p}{I_cR_J(I_0)} = \frac{\Phi_0 f_p}{I_cR_{shunt}} + \frac{\Phi_0 f_p}{I_cR_{QP}^{(eff)}(I_0)}. \tag{30}$$

In this equation, I_c is given by J_cS and $R_{QP}^{(eff)}(I_0)$ is proportional to S^{-1}, so the curve $\Phi_0 f_p/I_cR_{QP}^{(eff)}(I_0)$ as a function of I_0 does not depend on S. Furthermore, when the I_0 is just equal to the critical current I_c, the voltage $I_cR_{QP}^{(eff)}(I_c)$ is equal to V_{jump}, which is a universal constant for BSCCO, so that the dimensionless curve $\Phi_0 f_p/I_cR_{QP}^{(eff)}(I_0)$ becomes a universal curve $\mu(i_0)$ as a function of not the I_0 but the $i_0(\equiv I_0/I_c)$. Namely, the McCumber parameter for no shunt case also becomes a universal curve of i_0 and is given by $1/\mu^2(i_0)$ $[\equiv\beta_c^{(NS)}(i_0)]$. The universal curve $\mu(i_0)$ is shown in Fig. 1 as a function of i_0. For example, Fig. 1 shows that $\mu(0) = 1.8031\times10^{-3}$, $\mu(1) = 9.0154\times10^{-3}$, $\mu(2) = 1.4213\times10^{-2}$ and $\mu(3) = 1.9123\times10^{-2}$, thus, $\beta_c^{(NS)}(0) = 3.076\times10^5$, $\beta_c^{(NS)}(1) = 1.230\times10^4$, $\beta_c^{(NS)}(2) = 4.950\times10^3$, and $\beta_c^{(NS)}(3) = 2.734\times10^3$. The normalized current equation (28) is rewritten as

$$\frac{d^2\varphi(\tau)}{d\tau^2} + 2\pi\left(\frac{f_p}{f_r}\right)\frac{1}{\sqrt{\beta_c(i_0,J_c,SR_{shunt})}}\frac{d\varphi(\tau)}{d\tau} + (2\pi)^2\left(\frac{f_p}{f_r}\right)^2\{i_{CP}(\tau) - i_{ext}(\tau)\} = 0,$$

$$\frac{1}{\sqrt{\beta_c(i_0,J_c,SR_{shunt})}} = \lambda(J_c,SR_{shunt}) + \mu(i_0),$$

$$\lambda(J_c,SR_{shunt}) = \frac{\Phi_0 f_p}{J_c SR_{shunt}},$$

$$\mu(i_0) = \frac{1}{\sqrt{\beta_c^{(NS)}(i_0)}},$$

$$i_{ext}(\tau) = i_0 + i_r \sin 2\pi\tau + i_{noise}(\tau). \tag{31}$$

The nature of Shapiro steps can be understood by solving Eq. (31). In order to do so, first we set the values of i_r and f_r, i.e., fix the power and frequency of the external ac modulation, and then solve Eq. (31) for a given $i_0(\equiv\langle I_{ext}(t)\rangle_t/I_c)$; that is, for the amplitude of the external dc current, and finally, calculate the time average $\langle V(t)\rangle_t(\equiv V_{dc})$ of the voltage $V(t)$ given by $(\hbar/2e)d\varphi(t)/dt$ and get the dc I-V characteristics $V_{dc}(i_0)$.

For the modulation frequency f_r, there is a chaotic region defined by Eq. (3) in which Shapiro steps are not observed. The lower frequency f_{RC} can be rewritten as $1/2\pi R_J(I_0)C$, therefore, from Eq. (21) we get $f_{RC}=1/2\pi R_{QP}^{(eff)}(I_0)C + 1/2\pi R_{shunt}C$. The product $R_{QP}^{(eff)}(I_0)C$ at $I_0=I_c$ is equal to $V_{jump}C/I_c=V_{jump}\varepsilon\varepsilon_0/J_c d$, which is a universal constant. Therefore, the frequency $1/2\pi R_{QP}^{(eff)}(I_0)C$ for no shunt case also becomes a universal curve $f_{RC}^{(NS)}(i_0)$ as a function of i_0.

This curve is shown in Fig. 1 together with the universal curve $\mu(i_0)$. This figure shows that $f_{RC}^{(NS)}(0)=0.22$ GHz, $f_{RC}^{(NS)}(1)=1.10$ GHz, $f_{RC}^{(NS)}(2)=1.74$ GHz, and $f_{RC}^{(NS)}(3)=2.33$ GHz as examples. The lower frequency f_{RC} of the chaotic region is given by

$$f_{RC} = f_{RC}^{(NS)}(i_0) + f_{RC}^{(shunt)}(SR_{shunt}),$$

$$f_{RC}^{(shunt)}(SR_{shunt}) = \frac{1}{2\pi R_{shunt}C}. \tag{32}$$

Here it is noted that the ratio $f_{RC}^{(NS)}(i_0)/\mu(i_0)$ is the plasma frequency f_p, which is a universal constant, so that two universal curves (a) and (b) in Fig. 1 are curves whose ratio is a constant with the value of f_p.

The time average $\langle V(t)\rangle_t$ of voltage $V(t)$ is given by

$$\langle V(t)\rangle_t = \frac{1}{t_2-t_1}\int_{t_1}^{t_2} V(t)dt = \frac{\Phi_0 f_r}{2\pi(\tau_2-\tau_1)}\int_{\tau_1}^{\tau_2}\frac{d\varphi(\tau)}{d\tau}d\tau = \frac{\Phi_0 f_r}{2\pi}\frac{\varphi(\tau_2)-\varphi(\tau_1)}{\tau_2-\tau_1}, \tag{33}$$

where $\tau_j=f_r t_j (j=1,2)$. By the way, the period of the external ac modulation $i_r \sin 2\pi\tau$ is 1 for the dimensionless time τ. Therefore, in order to get an averaged value as correctly as possible, both the τ_1 and τ_2 in Eq. (33) must be integers. This is a very important point to get a good averaged value on the present numerical calculations. This is just a reason why we have defined the dimensionless time τ by $\omega_r t/2\pi$. The time interval t_2-t_1 must be large enough to get a well averaged value. We found that the well averaged value is obtained by setting t_1 and t_2 to 0.01 and 0.02 μs. The reader may think that the time interval with the value of 0.01 μs is small, but we must remember that the absolute time resolution Δt is 10 fs. Namely, the time interval 0.01 μs is equal to $\Delta t \times 10^6$, therefore, it should be mentioned that an averaged value is calculated by using all values from 1×10^6 to 2×10^6 calculation steps.

We are now interested in the sample condition to observe Shapiro steps clearly and stably. If no shunt case, i.e., $R_{shunt}\to\infty$, is considered, then we have no way to control a sample. In the present paper, therefore, we consider the case including shunt resistance R_{shunt} added externally, so that not only the R_{shunt} but also the S become important sample parameters. By the way, as can be seen from Eqs. (31) and (32), it is clear that the same SR_{shunt} product leads to a same result. The junction cross section S is controllable very well, but it is not so easy to control the value of R_{shunt}. The shunt resistance is usually made by evaporating the metal such as gold, so it is expected that the R_{shunt} is not so large. In the following, therefore, we consider a junction with $S=25$ μm^2 and adopt 1, 2, and 5 Ω as the values of R_{shunt}, tentatively. The capacitance C is calculated as 1.291 pF, so that the frequency $f_{RC}^{(shunt)}(SR_{shunt})$ defined by Eq. (32) is calculated as 123.3, 61.64, and 24.66 GHz for $SR_{shunt}=25$, 50, and 125 μm^2 Ω, respectively. The fact that the frequency $f_{RC}^{(shunt)}(25)$ is larger than the plasma frequency $f_p=122$ GHz means that there is no chaotic region in this case, i.e., the McCumber parameter β_c as a function of I_0 is always less than 1 for this case.

IV. RESULTS AND DISCUSSION

A. Effect of noise

In order to see the effect of noise, we consider here a sample with a condition of $S=25$ μm^2 and $R_{shunt}=1$ Ω. The reason why we have selected this sample condition is that the chaotic behavior is not observed in this sample so that we can see the effect of noise directly. The aim of this subsection is to see the effect of noise on the dc I-V characteristics. Thus, in the following, we evaluate the $i_{CP}(\tau)$ as $\sin\varphi(\tau)$ for simplicity and fix the value of amplitude i_r to 1. As can be seen from Eq. (31), the effect of the external current $i_{ext}(\tau)$ on observing the Shapiro steps is enhanced when $f_p/f_r>1$ and suppressed when $f_p/f_r<1$, so that the numerical calculations must be done for these two cases. The dc I-V characteristics with and without the noise calculated for $f_r=20$ GHz are shown in Figs. 2(a) and 2(b), and those for $f_r=200$ GHz are shown in Figs. 3(a) and 3(b). From the dc I-V characteristics shown in Figs. 2(a) and 2(b), we can see

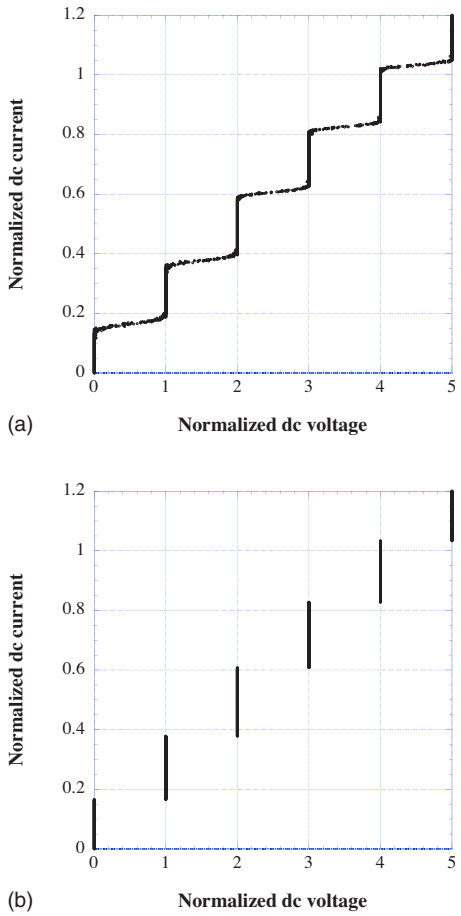

FIG. 2. (Color online) The dc *I-V* characteristics calculated for the case that the frequency f_r of external ac modulation is 20 GHz, the cross section S of the junction is 25 μm^2, the shunt resistance R_{shunt} added externally is 1 Ω, and the normalized amplitude i_r defined by I_r/I_c is 1, where I_r is the real amplitude of the external ac modulation and I_c is the the critical current of the Josephson junction. The horizontal axis indicates the normalized dc voltage defined by $\langle V(t)\rangle_t/\Phi_0 f_r$ and the vertical one shows the normalized dc current i_0 defined by I_0/I_c, where $\langle V(t)\rangle_t$ is the time averaged voltage defined by Eq. (33), Φ_0 is a flux quantum, and I_0 is the external dc current. The value of f_r is 20 GHz so that the voltage $\Phi_0 f_r$ is calculated as 41.357 μV, and S is 25 μm^2 so that the I_c is equal to 250 μA because of J_c=1000 A/cm^2. (a) is the case including noise defined by Eq. (20), and (b) is not.

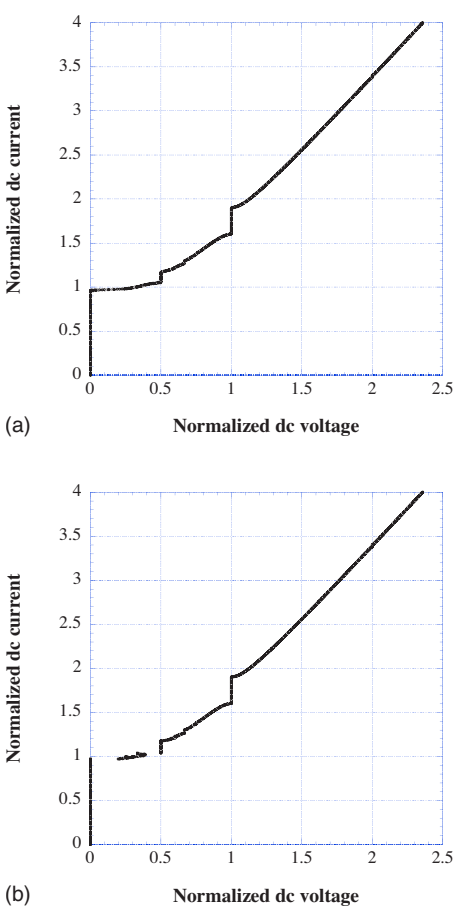

FIG. 3. (Color online) Calculated dc *I-V* characteristics. Except for the frequency f_r of external ac modulation, the calculation condition in this figure is the same as that in Fig. 2. The value of f_r is set to 200 GHz, so that the voltage $\Phi_0 f_r$ is 413.57 μV. Note that the junction cross section S is 25 μm^2 so that the I_c is 250 μA again. (a) is the case including noise and (b) is not.

that the effect of noise is observed but is not so large even in the case of f_r=20 GHz, i.e., in the case of f_p/f_r=122/20 $>$1. This fact means that the effect of noise is negligibly small in the case of $f_p/f_r<1$. Actually, we can see that there is no significant difference between the dc *I-V* characteristics shown in Figs. 3(a) and 3(b), in which the ratio f_p/f_r is equal to 122/200$<$1.

In the following calculations, we always take into account the effect of noise, because all the experiments always include the noise. Nevertheless, the conclusion obtained in this subsection says that the effect of noise is not so crucial for the Shapiro steps observed on an intrinsic Josephson junction in BSCCO at 4.2 K.

B. Evaluation of normalized CP tunneling current

The kernel $\kappa_{CP}(\tau-\tau')$ given by Eq. (18) is evaluated by two ways: one is the treatment based on the coherent tunneling denoted as $\kappa_{CP}^{(coh)}(\tau-\tau')$ and the other is the incoherent one $\kappa_{CP}^{(inc)}(\tau-\tau')$, so that the kernel $K_{CP}(\tau-\tau')$ in Eq. (14) is also written as $K_{CP}^{(coh)}(\tau-\tau')$ for coherent tunneling and $K_{CP}^{(inc)}(\tau-\tau')$ for incoherent one. By using the kernels, we can calculate the $i_{CP}(\tau)$'s, which are denoted as $i_{CP}^{(coh)}(\tau)$ and $i_{CP}^{(inc)}(\tau)$. The simplest expression for the $i_{CP}(\tau)$ is $\sin\varphi(\tau)$, so that the $i_{CP}^{(coh)}(\tau)$ and the $i_{CP}^{(inc)}(\tau)$ can be represented as

$$i_{CP}^{(coh)}(\tau) = \sin\varphi(\tau) + \Delta i_{CP}^{(coh)}(\tau),$$

$$i_{CP}^{(inc)}(\tau) = \sin\varphi(\tau) + \Delta i_{CP}^{(inc)}(\tau). \quad (34)$$

The phase difference $\varphi(\tau)$ is obtained by solving Eq. (31), so it is noted that the $\varphi(\tau)$ is a function of not only τ but also f_p, f_r, J_c, S, R_{shunt}, i_0, i_r, and T. Therefore, all the functions in Eq. (34) are also functions consisting of all variables mentioned now. Both the kernels $K_{CP}^{(coh)}(\tau-\tau')$ and $K_{CP}^{(inc)}(\tau-\tau')$ satisfy the normalization condition defined by Eq. (16), so it

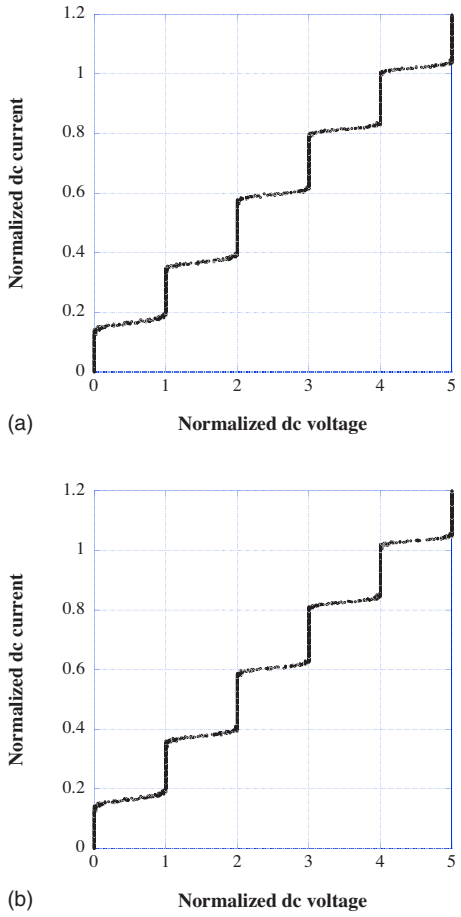

FIG. 4. (Color online) The dc *I-V* characteristics (a) and (b) calculated by using kernels $K_{CP}^{(coh)}(\tau-\tau')$ and $K_{CP}^{(inc)}(\tau-\tau')$. The calculation condition for (a) and (b) is the same as in Fig. 2(a); that is, $f_r=20$ GHz, $S=25$ μm^2, $R_{shunt}=1$ Ω, $i_r=1$, and the noise included. The horizontal axis indicates the normalized dc voltage $\langle V(t)\rangle_t/\Phi_0 f_r$ and the vertical one shows the normalized dc current i_0.

is reasonable to suppose that the magnitudes of the currents $\Delta i_{CP}^{(coh)}(\tau)$ and $\Delta i_{CP}^{(inc)}(\tau)$ are small. As can be seen from Eq. (31), the effect of $i_{CP}(\tau)$ is also enhanced in the case of $f_p/f_r>1$ and suppressed when $f_p/f_r<1$.

The dc *I-V* characteristics calculated by using kernels $K_{CP}^{(coh)}(\tau-\tau')$ and $K_{CP}^{(inc)}(\tau-\tau')$ are shown in Figs. 4(a) and 4(b). The calculation condition for the results in Fig. 4 is the same as in Fig. 2, i.e., $f_r=20$ GHz, $S=25$ μm^2, $R_{shunt}=1$ Ω, $i_r=1$, and $T=4.2$ K. We can see that even in the case of $f_p/f_r>1$, there is no considerable difference between the dc *I-V* characteristics shown in Figs. 4(a) and 4(b) and Fig. 2(a). Shapiro steps are observed on the quasiparticle (QP) branch of the dc *I-V* characteristics, so it is reasonable to conclude that the Shapiro steps are not sensitive to the nature of CP tunneling current. In other words, the experiment of Shapiro steps is not plausible as a tool to clarify the CP tunneling mechanism. By using the kernels $K_{CP}^{(coh)}(\tau-\tau')$ and $K_{CP}^{(inc)}(\tau-\tau')$ for $f_r=200$ GHz, i.e., $f_p/f_r<1$, we have calculated the dc *I-V* characteristics for coherent and incoherent cases and found that there are no significant differences between those characteristics, as is expected. Moreover, we

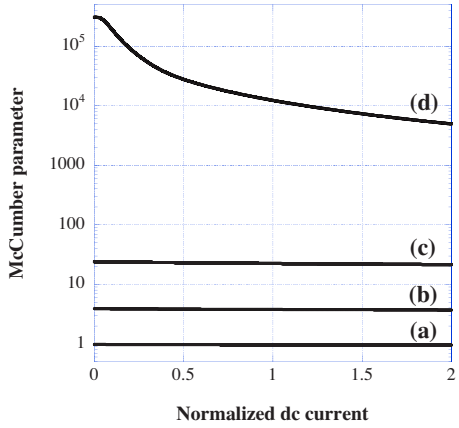

FIG. 5. (Color online) McCumber parameters $\beta_c(i_0,J_c,SR_{shunt})$ as a function of the normalized dc current i_0 defined by Eq. (31), where the critical current density J_c has been set to 1000 A/cm^2. Curves (a), (b), and (c) are those for $SR_{shunt}=25$, 50, and 125 μm^2 Ω. For example, the values of $\beta_c(0,1000,25)$, $\beta_c(0,1000,50)$, and $\beta_c(0,1000,125)$ are 0.977, 3.90, and 24.1 and those of $\beta_c(2,1000,25)$, $\beta_c(2,1000,50)$, and $\beta_c(2,1000,125)$ are 0.954, 3.71, and 21.4, respectively. For the comparison, the McCumber parameter $\beta_c^{(NS)}(i_0)$ for no shunt resistance, which is a universal curve as a function of only i_0, are also shown as (d).

have found that those dc *I-V* characteristics fairly well coincide with that shown in Fig. 3(a).

The general calculations for the $i_{CP}(\tau)$ using kernels $K_{CP}^{(coh)}(\tau-\tau')$ and $K_{CP}^{(inc)}(\tau-\tau')$ need very large CPU times. In this subsection, fortunately, we have found that the effect of currents $\Delta i_{CP}^{(coh)}(\tau)$ and $\Delta i_{CP}^{(inc)}(\tau)$ defined in Eq. (34) is not so crucial on the calculations of the dc *I-V* characteristics. In the following, therefore, we evaluate the $i_{CP}(\tau)$ as $\sin\varphi(\tau)$ to save CPU time.

C. SR_{shunt}-product dependence

The junction cross section S is set to 25 μm^2 and the external shunt resistances R_{shunt} of 1, 2, and 5 Ω are selected, so that the frequencies $f_{RC}^{(shunt)}(SR_{shunt})$ defined by Eq. (32) are 123.3, 61.64, and 24.66 GHz for $SR_{shunt}=25$, 50, and 125 μm^2 Ω, respectively. The $f_{RC}^{(NS)}(i_0)$ is small as can be seen from Fig. 1(b), therefore, the lower frequency f_{RC} of the chaotic region defined by Eq. (32) can be well approximated by $f_{RC}^{(shunt)}(SR_{shunt})$. In the following calculations, we adopt 20, 50, 100, 122, and 200 GHz as the external modulation frequency f_r. The dependence for the amplitude i_r of external modulation is discussed in the next subsection, so in this subsection the i_r is fixed to 1 again.

The McCumber parameters $\beta_c(i_0,J_c,SR_{shunt})$ with $J_c=1000$ A/cm^2 calculated for $SR_{shunt}=25$, 50, and 125 μm^2 Ω are shown in Figs. 5(a)–5(c) as a function of i_0. For comparison, the $\beta_c^{(NS)}(i_0)$ for no shunt case is also shown in Fig. 5(d). Note that the $\beta_c^{(NS)}(i_0)$ is a universal curve as a function of only i_0. The dc *I-V* characteristics calculated for $f_r=20$, 50, 100, 122, and 200 GHz are shown in Figs. 6–10, respectively, and the results calculated for $SR_{shunt}=25$, 50, and 125 are denoted as (a), (b), and (c) in the respective figures.

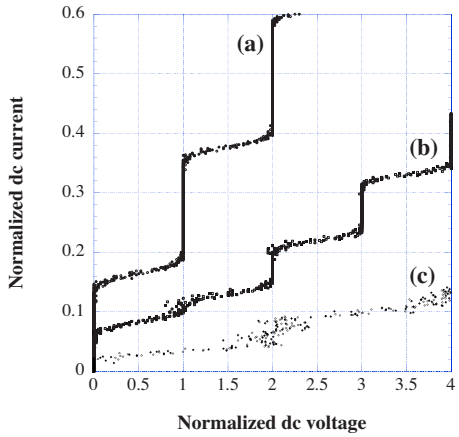

FIG. 6. (Color online) The dc *I-V* characteristics calculated for the case that $f_r=20$ GHz, $S=25$ μm^2, and $i_r=1$. The dc *I-V* characteristics when $R_{shunt}=1$, 2, and 5 Ω are denoted as (a), (b), and (c), respectively. Note that all the calculations include the noise. The horizontal axis indicates the normalized dc voltage $\langle V(t)\rangle_t/\Phi_0 f_r$ and the vertical one shows the normalized dc current i_0. The $\Phi_0 f_r$ is 41.357 μV.

First, from the calculated results for the sample with a condition of $SR_{shunt}=25$ μm^2 Ω, we can see that the sample always shows clear Shapiro steps for all the frequencies we adopted. This is natural since the McCumber parameter of this sample is always less than 1, as can be seen from Fig. 5(a). Therefore, if a sample with $SR_{shunt}\leqslant 25$ μm^2 Ω is made using BSCCO, it is expected that its sample works well as a Shapiro step device. Next, the calculated results for the sample with $SR_{shunt}=50$ μm^2 Ω show that except for the case of $f_r=200$ GHz, its sample is not so good as a Shapiro step device, especially, as the device based on the first-order Shapiro step observed on the voltage $\Phi_0 f_r$, and finally, the calculated results for $SR_{shunt}=125$ μm^2 Ω show that its sample cannot be used as a Shapiro step device, except for the case of $f_r=200$ GHz. It is natural since $f_r>f_p$ for all samples. As already noted, it is easy to make a shunt resistance but is hard to control the value of the resistance R_{shunt} correctly. The results for $f_r\leqslant f_p$ shown in Figs. 6–9 clearly show that a slight change of R_{shunt} makes a large change of the dc *I-V* characteristics. This high-sensitivity for the R_{shunt} is not acceptable as a device, because the device must be stable for *unexpected* external disturbances. On the contrary to the results for $f_r\leqslant f_p$, the results for $f_r>f_p$ shown in Fig. 10 show that the clear first-order Shapiro step is observed for all the resistances. Therefore, it is concluded that the device operated on the condition of $f_r>f_p$ is stable as compared with that of $f_r\leqslant f_p$.

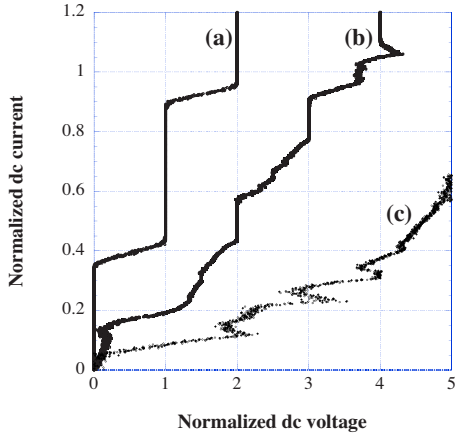

FIG. 7. (Color online) The same as in Fig. 6 but for $f_r=50$ GHz. The $\Phi_0 f_r$ is 103.39 μV.

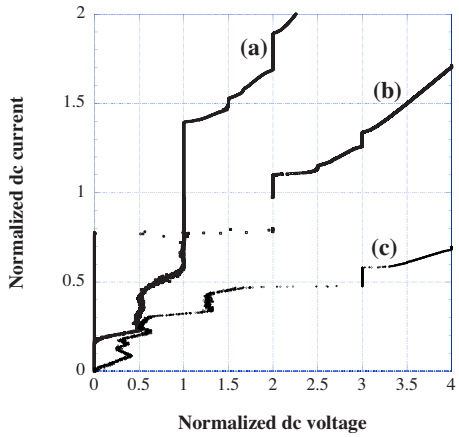

FIG. 8. (Color online) The same as in Fig. 6 but for $f_r=100$ GHz. The $\Phi_0 f_r$ is 206.78 μV.

D. i_r dependence

The height ΔI_n of the nth-order Shapiro step observed on the voltage $n\Phi_0 f_r$ ($n=\pm 1,\pm 2,\ldots$) depends on the power of the external ac modulation with the frequency f_r. The square root of power is proportional to the amplitude I_r of the external ac modulation, so in the following, we consider the i_r dependence of $\Delta i_n(\equiv \Delta I_n/I_c)$, i.e., $\Delta i_n(i_r)$. In the practical calculations, three samples with $SR_{shunt}=25$, 50, and 125 μm^2 Ω are selected again, and f_r of 20 and 200 GHz are adopted. The $\Delta i_n(i_r)$ calculated for $f_r=20$ and 200 GHz are shown in Figs. 11 and 12, respectively. In those figures, (a), (b), and (c) are the $\Delta i_n(i_r)$ calculated for $SR_{shunt}=25$, 50, and

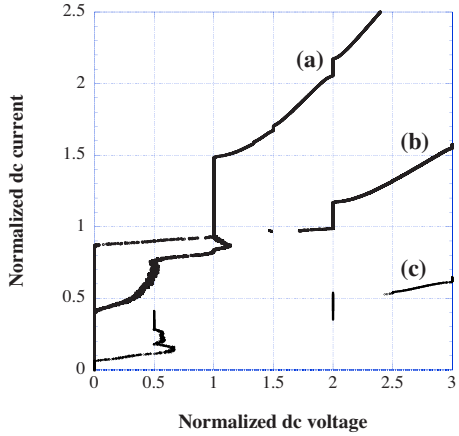

FIG. 9. (Color online) The same as in Fig. 6 but for $f_r=122$ GHz, which is the plasma frequency f_p of an intrinsic Josephson junction in BSCCO at 4.2 K. The $\Phi_0 f_r$ is 252.28 μV.

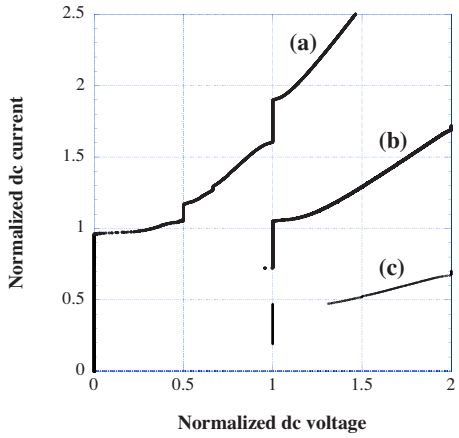

FIG. 10. (Color online) The same as in Fig. 6 but for f_r =200 GHz. The $\Phi_0 f_r$ is 413.57 μV.

125 $\mu m^2\,\Omega$. By the way, according to the simplest voltage biased model, the Shapiro step height Δi_n varies as a Bessel functional. For comparison, therefore, the absolute values of Bessel functions $J_n(x)$ with $n=0$, 1, and 2 are also shown in Figs. 11 and 12 as a function of x. Here note that the $|J_n(x)|$ is adjusted for the x so as to nearly fit the present $\Delta i_0(i_r)$. Figures 11(a)–11(c) for $f_r=20$ GHz indicate that only the sample with $SR_{shunt}=25$ $\mu m^2\,\Omega$ shown in (a) can be used as a Shapiro step device operating on the wide range of i_r, and Figs. 12(a)–12(c) for $f_r=200$ GHz clearly show that all three samples can be used as a Shapiro step device for the wide range of i_r. Moreover, Figs. 11 and 12 show that when f_r =20 GHz, the i_r dependence of the $\Delta i_n(i_r)$ with $n\neq 0$ largely differs from the Bessel functional behavior, but that of f_r =200 GHz is not so far from the Bessel one. From the above, we can conclude that the Shapiro step device ought to operate on a condition $f_r > f_p$ rather than $f_r < f_{RC}$.

The plasma frequency f_p is given by $\sqrt{J_c d/2\pi\Phi_0\varepsilon\varepsilon_0}$. Using the method of the thermodynamic Green's functions, Ambegaokar and Baratoff[24] have presented a general expression for the Josephson tunneling current $I_c(T)$ as a function of temperature T. Thus, the temperature dependent critical current density $J_c(T)$ is written as

$$J_c(T) = \frac{2e}{S\hbar}\sum_{\mathbf{k}}^{BZ_1}\sum_{\mathbf{k}'}^{BZ_1}|H'_{\mathbf{k},\mathbf{k}'}|^2\frac{|\Delta_{\mathbf{k}}\Delta_{\mathbf{k}'}|}{E_{\mathbf{k}}E_{\mathbf{k}'}}\left[\frac{f(E_{\mathbf{k}})-f(E_{\mathbf{k}'})}{E_{\mathbf{k}}-E_{\mathbf{k}'}} + \frac{1-f(E_{\mathbf{k}})-f(E_{\mathbf{k}'})}{E_{\mathbf{k}}+E_{\mathbf{k}'}}\right]. \quad (35)$$

Note that Eq. (35) corresponds to the denominator of Eq. (18). Here, the $H'_{\mathbf{k},\mathbf{k}'}$ is the matrix element due to the $\mathbf{k}\rightarrow\mathbf{k}'$ tunneling, so that the amplitude of the matrix element strongly depends on the nature of an insulating layer in BSCCO. The ε and d are dielectric constant and the thickness of the insulating layer, so that the value of plasma frequency f_p is largely affected by the nature of the insulating layer in BSCCO.

It is well known that by doping Pb atoms into the BSCCO single crystals, Bi atoms, which make BiO insulating tunnel barriers in BSCCO, are substitutionally replaced by Pb atoms, and as a result, $(Bi_{1-x}Pb_x)_2Sr_2CaCu_2O_{8+\delta}$ (BPSCCO) high-T_c superconductors are synthesized, that is, the Pb atom works as an atom to control the properties of the insulating barrier in BSCCO.[25] Actually, it has been observed that the Pb doping makes a structural change of the insulating layer, such as a change from the Bi-type incommensurate modulation structure to the Pb-type commensurate one and the critical current density J_c rapidly increases with increasing the value of x identified as the Pb concentration.[25,26] The experiment done by Irie *et al.* showed that the J_c at $x=0$, 0.15, and 0.2 are about 1, 10, and 17.5 kA/cm^2, respectively.[27] In the next section, therefore, we consider the J_c dependence of Shapiro steps observed on a condition $f_r > f_p$.

E. J_c dependence

In this section, J_c's of 1, 5, and 10 kA/cm^2 are adopted so that the corresponding f_p are calculated as 122, 273, and 386 GHz, respectively. We consider here the case of $f_r > f_p$ so that f_r of 760 GHz is adopted, because there is an excellent experiment for Shapiro steps done by Wang *et al.*[15] in which a microwave at 760 GHz from a far-infrared laser has been used for the BSCCO with no shunt resistance. We will see later that a large power of the external ac modulation is needed to reproduce the Shapiro steps observed by Wang *et al.* in which no resistively shunted and no Pb-doped BSCCO sample has been used. We focus our attention to the J_c dependence so that the normalized amplitude i_r of the external modulation is set to 1 and the cross section S of the junction is set to 25 μm^2 again.

The dc I-V characteristics calculated for $J_c=1$ kA/cm^2, i.e., Pb-undoped BSCCO, are shown in Fig. 13, in which curves (a), (b), and (c) correspond to $R_{shunt}=1$, 2, and 5 Ω, and for comparison, the no shunt case is drawn by curve (d). The ratio f_p/f_r on the present case is small such as 0.16, so it is supposed that the effect of i_r is suppressed as can be seen from Eq. (31). Actually, Fig. 13 shows that there are no detectable Shapiro steps in the case of $i_r=1$ and J_c =1 kA/cm^2. Note that the real amplitude I_r of the external ac modulation is given by $i_r I_c$ so that the I_r for the present case is 250 μA. The dc I-V characteristics calculated for $i_r=10$ and $J_c=1$ kA/cm^2, i.e., the I_r is 2.5 mA and the power is a hundred times larger than that of $i_r=1$, are shown in Fig. 14. Figure 14 shows that there are detectable Shapiro steps and the real heights ΔI_1 of the first-order Shapiro step are calculated as 65, 63, 63, and 30 μA for (a), (b), (c), and (d), respectively. The dc I-V characteristics calculated for $J_c=5$ and 10 kA/cm^2 are shown in Figs. 15 and 16, where we note that the normalized amplitude i_r of the external ac modulation has been set to 1 so that the real amplitudes I_r are 1.25 and 2.5 mA for Figs. 15 and 16, respectively. Figures 15 and 16 show that increasing the J_c, i.e., the f_p, makes a clear Shapiro step even in the case of $i_r=1$. From Fig. 15, the real heights ΔI_1 of the first-order Shapiro step are calculated as (a) 163, (b) 163, (c) 138, and (d) 88 μA, and Fig. 16 shows that the ΔI_1 is 625, 550, 425, and 325 μA for (a), (b), (c), and (d), respectively. It should be emphasized that the real height ΔI_1 calculated for $J_c=10$ kA/cm^2 and $i_r=1$ is about

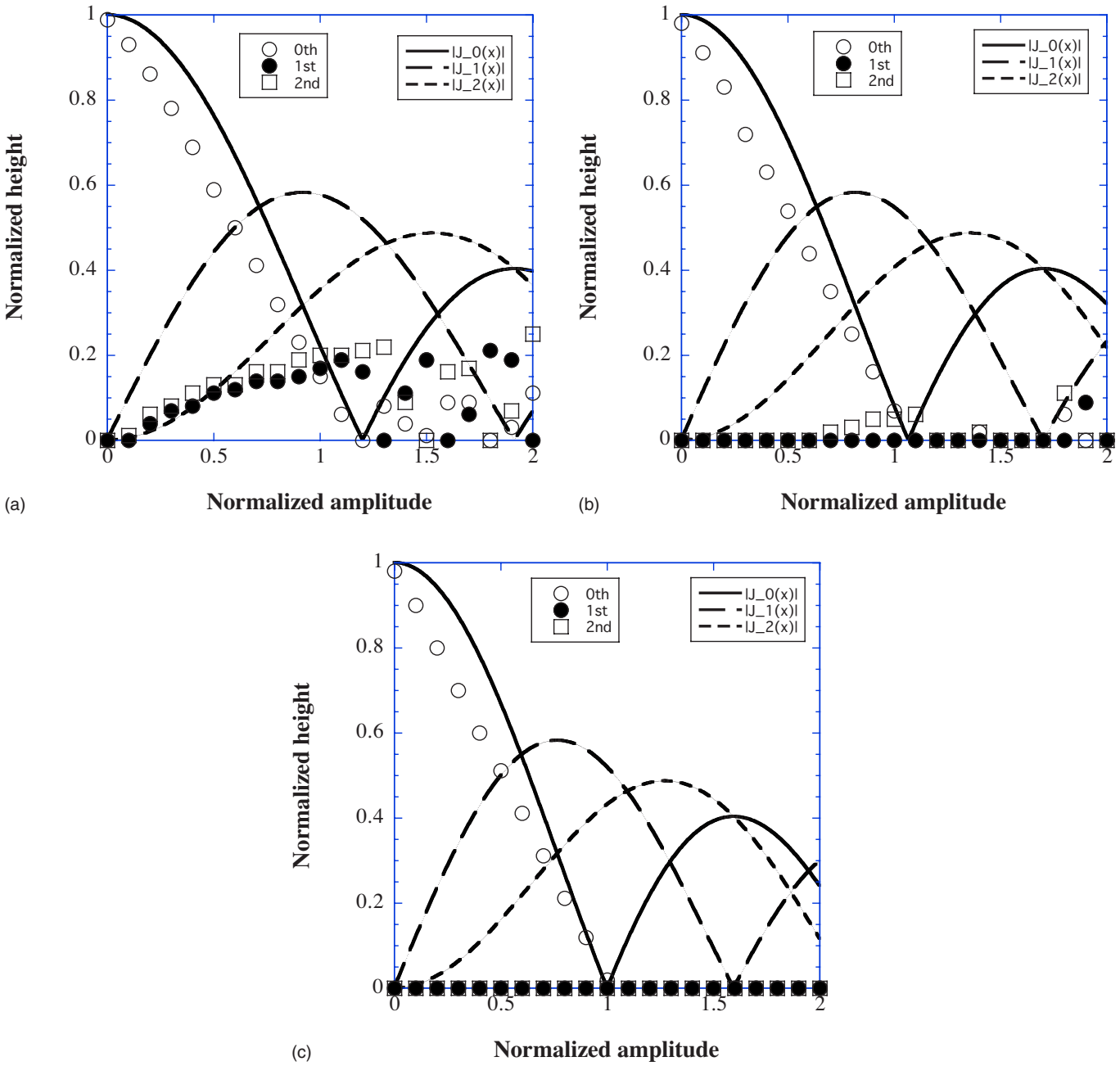

FIG. 11. (Color online) Normalized height $\Delta i_n(i_r)[\equiv \Delta I_n(i_r)/I_c]$ of the nth-order Shapiro step as a function of the normalized amplitude $i_r(\equiv I_r/I_c)$ of the external ac modulation where $0 \leqslant i_r \leqslant 2$. The frequency f_r of the external ac modulation is 20 GHz, and the value of the SR_{shunt} product is (a) 25, (b) 50, and (c) 125 $\mu m^2\ \Omega$. For comparison, the absolute values of Bessel functions $J_n(x)$ with $n=0$, 1, and 2 are also shown. Note that the height $\Delta i_n(i_r)$ with $n \neq 0$ is due to Shapiro steps but that with $n=0$ corresponds to the normalized critical current as a function of i_r so that the height $\Delta i_0(i_r)$ is not due to the Shapiro step.

ten times larger than that for $J_c=1$ kA/cm^2 and $i_r=10$, in spite of the fact that the real amplitudes I_r used in both cases are equal to each other. This fact means that the Shapiro step device, which works well for the high frequency modulation such as 760 GHz and more, should be made from Pb-doped BSCCO single crystals rather than the undoped ones. In other words, in order to get a Shapiro step with a large real height ΔI_1 by using Pb-undoped BSCCO single crystals, a large power of external ac modulation is needed.

By using the coherent and incoherent kernels $K_{CP}^{(coh)}(\tau-\tau')$ and $K_{CP}^{(inc)}(\tau-\tau')$, for $f_r=760$ GHz, we have carried out the general calculations for the dc I-V characteristics on the condition such that $J_c=10$ kA/cm^2, $f_p=386$ GHz, $S=25\ \mu m^2$, $i_r=1$, and $R_{shunt}=1\ \Omega$, which is the same condition as in Fig. 16(a). Again we have found that the resultant dc I-V characteristics coincide with each other fairly well and there are no detectable differences between those characteristics and the dc I-V characteristics shown in Fig. 16(a).

In the present paper, we focused a single intrinsic Josephson junction (IJJ) in BSCCO consisting of a series array of IJJ's. Even in the case of no magnetic field, it is known that the interaction appears between the IJJ's when the charging

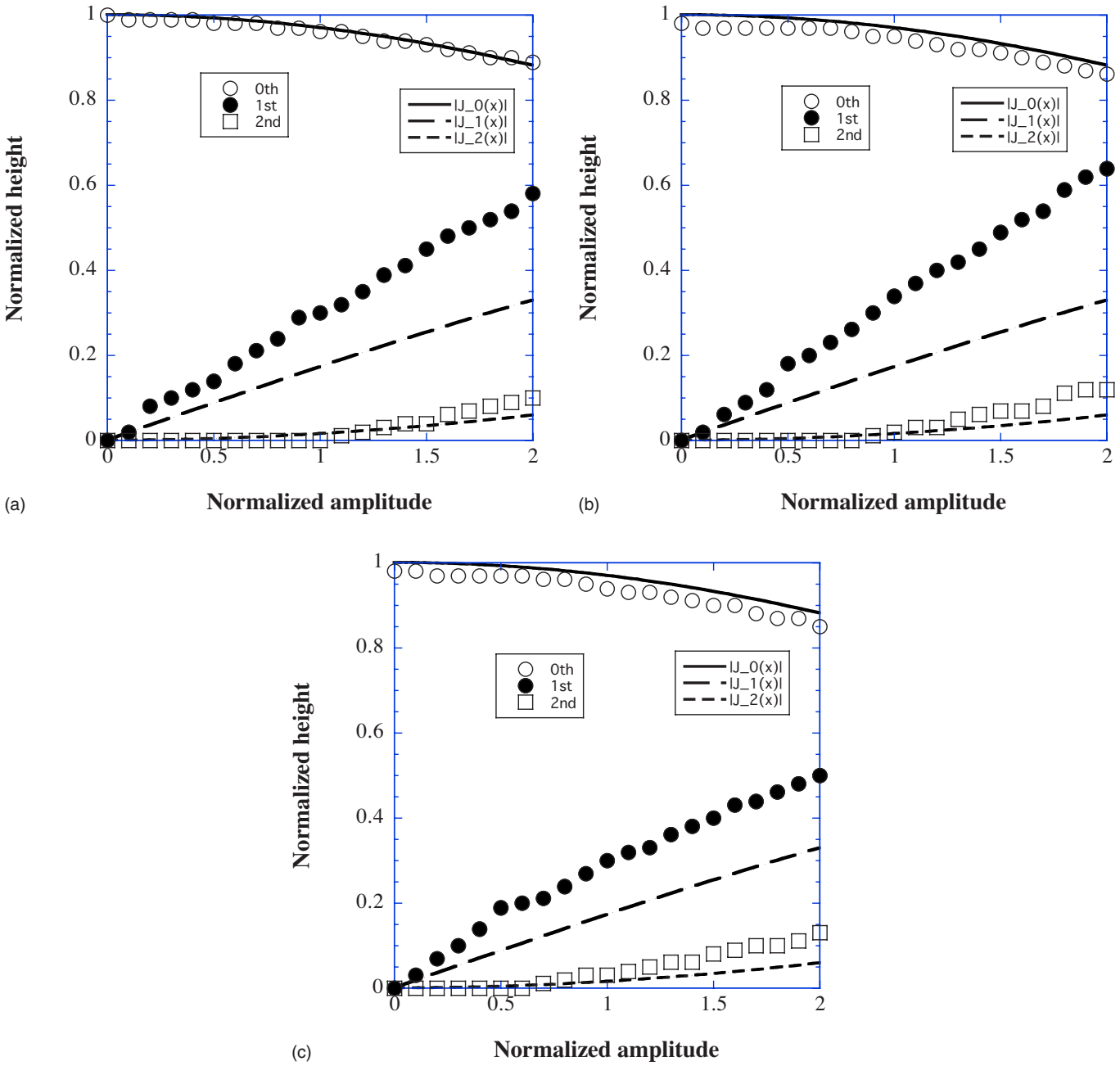

FIG. 12. (Color online) The same as in Fig. 11 but for f_r=200 GHz.

effect cannot be neglected. Actually, Rother *et al.* have pointed out that the charge imbalance effects make a voltage of the Shapiro step, which is observed as a downshift of 3% from the canonical value.[28] However, it is also known that if the current-biased case is considered, the resultant *I-V* characteristics are quite similar to those of the single junction systems.[29] We adopted here the current-biased case with no magnetic field, so that the present result is easily applicable to the *N*-IJJ's stacked system. Namely, if all the IJJ's show exactly the same character, the voltage observing Shapiro steps is simply *N* times larger than that of a single junction.

We have considered a junction with the size of 5 $\times$5 μm. Therefore, first it should be noted that no observation of the phenomena unique to a small sized junction could be expected. Next, the length L of the junction is 5 μm and the thickness d of the insulating layer is 12 Å, so that the magnetic induction B_0 needed to insert a flux quantum Φ_0 into a SIS-Josephson junction is calculated as 0.345 T. Therefore, when the external magnetic induction B_{ext} is larger than B_0, it seems that a considerable interaction between different junctions is found and the phase difference on the junction is understood by solving a coupled sine-Gordon equation with a matrix form. We have already simulated the voltex structures in a stack of five Josephson junctions using the coupled sine-Gordon equation with a matrix form, when an appropriate magnetic field has been applied.[30] In order to see how the fluxon dynamics affects the shape of Shapiro steps, we solved the coupled sine-Gordon equation

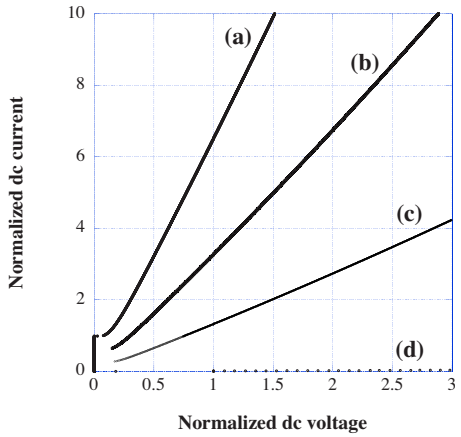

FIG. 13. (Color online) The dc *I-V* characteristics calculated for the case that $J_c=1$ kA/cm^2, $f_p=122$ GHz, $f_r=760$ GHz, $S=25$ μm^2, and $i_r=1$. The dc *I-V* characteristics when $R_{shunt}=1$, 2, and 5 Ω are denoted as (a), (b), and (c), respectively. Note that all the calculations include the noise. The horizontal axis indicates the normalized dc voltage $\langle V(t)\rangle_t/\Phi_0 f_r$ and the vertical one shows the normalized dc current i_0. The value of $\Phi_0 f_r$ is 1571.6 μV. The critical current I_c corresponding to $i_0=1$ is 250 μA because of $J_c=1$ kA/cm^2 and $S=25$ μm^2. For comparison, the dc *I-V* characteristics calculated for the no shunt case $R_{shunt}\rightarrow\infty$ is also shown as (d). The real amplitude I_r of the external ac modulation is 250 μA.

including the effect of magnetic field. The calculated results showed that the shape of Shapiro steps remains the same when the applied magnetic field is as small as $\sim 0.1B_0$. In the present work, we consider the case such that the effect of the magnetic field is negligible, that is, $B_{ext}\ll B_0$, so it is noted that both the interaction between the different junctions and the spatial variation of the phase difference can be ignored fairly well.

At the end of this section, we wish to make a regarding for the steps originating from the flux flow. It is well known

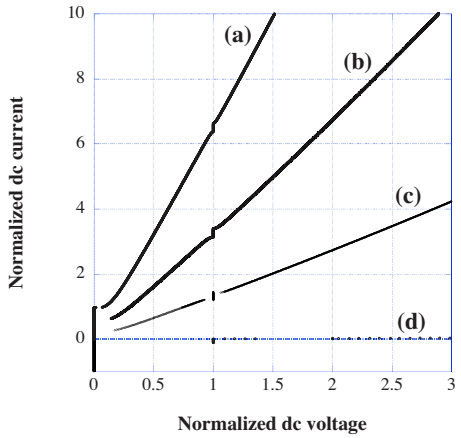

FIG. 14. (Color online) The same as in Fig. 13 but for $i_r=10$, thus, the real amplitude I_r is 2.5 mA. In (d), a small but a clear zero-crossing Shapiro step is observed on the first-order Shapiro step. The normalized height Δi_1 of the first-order Shapiro step is (a) 0.26, (b) 0.25, (c) 0.25, and (d) 0.12, therefore, the real height ΔI_1 given by $I_c\Delta i_1$ is equal to (a) 65, (b) 63, (c) 63, and (d) 30 μA, respectively.

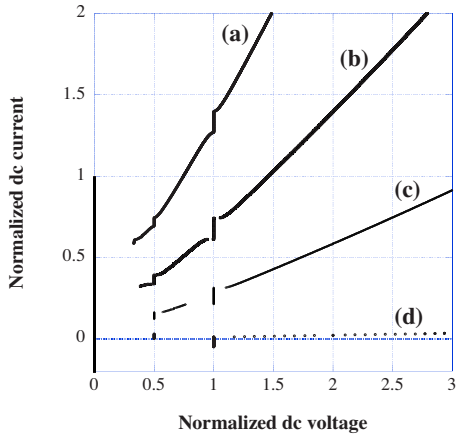

FIG. 15. (Color online) The same as in Fig. 13 but for $J_c=5$ kA/cm^2 and $f_p=273$ GHz. The critical current I_c is 1.25 mA so that the real amplitude I_r of the external ac modulation is 1.25 mA because of $i_r=1$. A zero-crossing Shapiro step is observed on the first-order Shapiro step in (d). The normalized heights Δi_1 for (a), (b), (c), and (d) are 0.13, 0.13, 0.11, and 0.07, thus, the real heights ΔI_1 are (a) 163, (b) 163, (c) 138, and (d) 88 μA, respectively.

that fluxons can be introduced into the Josephson junctions by an external ac modulation, and at low modulation frequency clear steps can be observed on the *I-V* characteristics. Actually, Irie and Oya have measured the *I-V* characteristics under the microwave irradiations with four frequencies 9.8, 11.6, 14.0, and 17.4 GHz, and concluded that the observed steps are not Shapiro steps but are considered to be the microwave induced flux-flow steps, because the voltages of those steps increase linearly with the square root of the microwave power but are independent of the external frequency.[31] Recently, Wang *et al.* did the experiment of the *I-V* characteristics for annular intrinsic Josephson junctions at low microwave frequency ($\sim$20 GHz), and observed clear

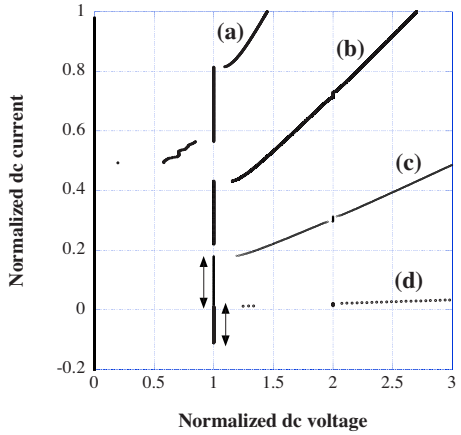

FIG. 16. (Color online) The same as in Fig. 13 but for $J_c=10$ kA/cm^2 and $f_p=386$ GHz. The critical current I_c is 2.5 mA so that the I_r is also equal to 2.5 mA. Note that the I_r of the present case is equal to that of the case in Fig. 14. A zero-crossing Shapiro step is observed on the first-order Shapiro step in (d). The normalized heights Δi_1 for (a), (b), (c) and (d) are 0.25, 0.22, 0.17, and 0.13, thus, the real heights ΔI_1 are (a) 625, (b) 550, (c) 425, and (d) 325 μA, respectively.

steps in the *I-V* curves.[18] They have ascribed these experimental facts to such that the rotation frequency of the fluxons trapped in annular intrinsic Josephson junctions could be locked to the external microwave frequency.[18] Wang *et al.* have called these steps Shapiro steps, but we think that those steps should be called the microwave induced flux-flow steps rather than Shapiro steps, because a coupling between the fluxon motion and the external microwave makes such steps.

V. SUMMARY

Shapiro steps observed on the superconductor-insulator-superconductor (SIS) Josephson junctions can be used as a quantum voltage standard and an incident microwave detecter. $Bi_2Sr_2CaCu_2O_{8+\delta}$ (BSCCO) high-T_c superconductors consist of a series array of the SIS intrinsic Josephson junctions, so that it may be possible to make a Shapiro step device using BSCCO single crystals. In the present paper, we have studied the conditions to observe the Shapiro steps clearly and stably on an intrinsic Josephson junction in BSCCO. In order to see those, we have rewritten the normalized current equation, which is valid for the general case such that the McCumber parameter is no longer a constant, and solved the current equation full numerically and got the phase shift $\varphi(t)$ as a function of time t. In the numerical calculations, the quasiparticle (QP) tunneling current has been evaluated by using the normalized *I-V* characteristics obtained from our model based on the *d*-wave symmetry superconducting gap and the Cooper-pair (CP) tunneling current has been calculated on the basis of the general way in which the coherent and incoherent CP tunneling currents can be correctly calculated within the framework of the *d*-wave symmetry superconducting gap. In addition to the calculations for the QP and CP tunneling currents, we have further taken into accout the effect of noise using normal random numbers.

We have shown that if no shunt resistance case is considered, i.e., the case that we have no way to control the sample condition, then the normalized current equation to be solved becomes an equation that depends on only a universal curve $\mu(i_0)$ as a function of the normalized dc current i_0 defined by I_0/I_c. Namely, we have pointed out that the normalized current equation for the no shunt case always gives a result irrespective of the sample condition. This nature is improved by introducing the shunt resistance R_{shunt}, which is added externally. One of the improvements is that the McCumber parameter becomes a parameter that does not have a large value and does not so strongly depend on i_0, on the contrary to no shunt case in which the McCumber parameter is very large and strongly depends on i_0. Namely, the large hysteretic behavior observed on the *I-V* characteristics in the no shunt resistance case is reduced by introducing the R_{shunt}. We have found that the BSCCO sample with no hysteretic structure is obtained when the SR_{shunt} product is less than 25 $\mu m^2\,\Omega$.

It is well known that the chaotic behavior is observed when the frequency f_r of the external ac modulation is between f_{RC} and f_p, where the f_{RC} is the frequency due to the *RC*-time constant given by Eq. (32) and the f_p is the plasma frequency of an intrinsic Josephson junction in BSCCO. We have found that the f_{RC} of no shunt case becomes a universal curve $f_{RC}^{(NS)}(i_0)$ as a function of only i_0 and its value locates around a low frequency region. Therefore, another improvement due to the addition of R_{shunt} is the increasing value of f_{RC}. We have shown that no chaotic behavior is observed on BSCCO when the SR_{shunt} product is less than 25 $\mu m^2\,\Omega$.

As can be seen from the normalized current equation (31), the effect of the external and CP currents $i_{ext}(\tau)$ and $i_{CP}(\tau)$ is exhanced when $f_p/f_r > 1$ and suppressed when $f_p/f_r < 1$. The $i_{ext}(\tau)$ includes the noise current $i_{noise}(\tau)$, and hence, first we have studied the effect of noise. As a result, we have found that the noise effect is observed in the case of $f_p = 122$ GHz and $f_r = 20$ GHz but is not so large even in the case of $f_p/f_r \simeq 6$, and that no noticeable noise effect is also observed in the case of $f_p = 122$ GHz and $f_r = 200$ GHz, as is expected.

In the present paper, we have presented a general way to evaluate the normalized CP current $i_{CP}(\tau)$ as a function of τ, i.e., time t. By using the general way, we have calculated $i_{CP}(\tau)$'s for the coherent and incoherent CP tunneling cases within the framework of the *d*-wave symmetry superconducting gap. From the calculations for $f_r = 20$, 200, and 760 GHz, we have found that the dc *I-V* characteristics calculated from the coherent and incoherent schemes well coincide with each other and those are very similar to that calculated using the simplest way in which $i_{CP}(\tau)$ is evaluated as $\sin\varphi(\tau)$.

We have pointed out that the SR_{shunt} product is an important parameter. By using three values 25, 50, and 125 $\mu m^2\,\Omega$ as the SR_{shunt} product, we have calculated the dc *I-V* characteristics for $f_r = 20$, 50, 100, 122, and 200 GHz. As a result, we have concluded that a Shapiro step device made from BSCCO single crystals works stably on the condition of $f_r > f_p$ rather than $f_r \leqslant f_{RC}$.

In order to see how the height ΔI_n of the *n*th-order Shapiro step depends on the amplitude I_r of the external ac modulation, we have calculated the normalized height $\Delta i_n (\equiv \Delta I_n / I_c)$ as a function of the normalized amplitude $i_r (\equiv I_r / I_c)$. We have found that good responses are obtained within the wide range of i_r when the Shapiro step device is operated on a condition of $f_r > f_p$.

The critical current density J_c is also an important parameter. The J_c value of BSCCO seems to *weakly* depend on the condition of sample preparations; that is, the so-called "laboratory dependence" seems to be found slightly. In the present paper, we have set the J_c value to 1 kA/cm^2 for simplicity and regarded it as a universal constant. This treatment may be true for pure BSCCO single crystals. It is experimentally known that the J_c value is increased by doping Pb atoms into the BSCCO single crystals. Therefore, we have checked the J_c dependence of the dc *I-V* characteristics and the resultant Shapiro steps. As the J_c increases, the plasma frequency f_p increases, and hence it is sure that the Shapiro step device made from the Pb-doped BSCCO single crystals works well in the high frequency range of the external ac modulation. We have found that the high frequency response is improved by an increase in J_c. Furthermore, we have found that the response for the high J_c junction is much better than that for the low one when an intrinsic Josephson junction is irradiated by the microwaves with the same power.

Finally, we wish to make a comment regarding the nonequilibrium effects. As those effects, the quasiparticle dis-

equilibrium could be considered[32–34] so-called μ^* and T^* models. Its effect makes a departure from the thermal equilibrium of the Fermi-Dirac distribution function, so that the critical current density $J_c(T)$ given by Eq. (35) could be changed by taking into account the effect of the quasiparticle disequilibrium. Since $f_p \propto \sqrt{J_c(T)}$, the plasma frequency f_p is changed to the effective plasma frequency f_p^*, thus the chaotic region, in which Shapiro steps cannot be observed, is also changed due to the inclusion of the quasiparticle disequilibrium. However, it should be noted that the *conditions* for observing Shapiro steps clearly and stably; that is, the shunt resistance is added into IJJ and the external ac modulation frequency f_r is higher than the effective plasma frequency f_p^*, remain the same even if the nonequilibrium effects are taken into account. Here note that the frequency ratio f_p^*/f_p is equal to $\sqrt{J_c(T^*)/J_c(T)}$ for the T^* model[33] and $\sqrt{J_c(\mu^*)/J_c(\mu)}$ for the μ^* one,[32] where T^* and μ^* are the effective temperature and chemical potential, respectively.

We believe that the present work works as a theoretical guideline for the Shapiro steps study on the intrinsic Josephson junctions in high-T_c cuprate superconductors.

[1] S. Shapiro, Phys. Rev. Lett. **11**, 80 (1963).
[2] R. Kleiner, F. Steinmeyer, G. Kunkel, and P. Müller, Phys. Rev. Lett. **68**, 2394 (1992).
[3] R. Kleiner and P. Müller, Phys. Rev. B **49**, 1327 (1994).
[4] G. Oya, N. Aoyama, A. Irie, S. Kishida, and H. Tokutaka, Jpn. J. Appl. Phys., Part 1 **31**, L829 (1992).
[5] A. Yurgens, D. Winkler, N. V. Zavaritsky, and T. Claeson, Phys. Rev. B **53**, R8887 (1996).
[6] Yu. I. Latyshev, J. E. Nevelskaya, and P. Monceau, Phys. Rev. Lett. **77**, 932 (1996).
[7] K. Schlenga, R. Kleiner, G. Hechtfischer, M. Mößle, S. Schmitt, P. Müller, Ch. Helm, Ch. Preis, F. Forsthofer, J. Keller, H. L. Johnson, M. Veith, and E. Steinbeiß, Phys. Rev. B **57**, 014518 (1998).
[8] A. Irie, Y. Hirai, and G. Oya, Appl. Phys. Lett. **72**, 2159 (1998).
[9] D. J. Van. Harlingen, Rev. Mod. Phys. **67**, 515 (1995).
[10] C. C. Tsuei and J. R. Kirtley, Rev. Mod. Phys. **72**, 969 (2000).
[11] A. Damascelli, Z. Hussain, and Z.-X. Shen, Rev. Mod. Phys. **75**, 473 (2003).
[12] Y. J. Doh, J. Kim, K. T. Kim, and H. J. Lee, Phys. Rev. B **61**, R3834 (2000).
[13] H. B. Wang, P. H. Wu, and T. Yamashita, Phys. Rev. Lett. **87**, 107002 (2001).
[14] Yu. I. Latyshev, M. B. Gaifullin, T. Yamashita, M. Machida, and Y. Matsuda, Phys. Rev. Lett. **87**, 247007 (2001).
[15] H. B. Wang, P. H. Wu, J. Chen, K. Maeda, and T. Yamashita, Appl. Phys. Lett. **80**, 1604 (2002).
[16] G. Oya, A. Terada, N. Takahashi, A. Irie, and T. Hashimoto, Jpn. J. Appl. Phys., Part 1 **44**, L491 (2005).
[17] G. Oya, T. Hashimoto, and A. Irie, Supercond. Sci. Technol. **19**, S191 (2006).
[18] H. B. Wang, S. M. Kim, S. Urayama, M. Nagao, T. Hatano, S. Arisawa, T. Yamashita, and P. H. Wu, Appl. Phys. Lett. **88**, 063503 (2006).
[19] M. Kitamura, A. Irie, and G. I. Oya, Phys. Rev. B **66**, 054519 (2002).
[20] A. Irie and G. Oya, Physica C **367**, 393 (2002).
[21] R. L. Kautz and R. Monaco, J. Appl. Phys. **57**, 875 (1985).
[22] A. Barone and G. Paterno, *Physics and Applications of the Josephson Effect* (Wiley, New York, 1982).
[23] Yu. I. Latyshev, T. Yamashita, L. N. Bulaevskii, M. J. Graf, A. V. Balatsky, and M. P. Maley, Phys. Rev. Lett. **82**, 5345 (1999).
[24] V. Ambegaokar and A. Baratoff, Phys. Rev. Lett. **10**, 486 (1963).
[25] G. Oya and A. Irie, Recent Res. Dev. Appl. Phys. **2**, 429 (1999).
[26] G. Oya and A. Irie, Physica C **293**, 149 (1997).
[27] A. Irie, T. Mimura, M. Okano, and G. Oya, Supercond. Sci. Technol. **14**, 1097 (2001).
[28] S. Rother, Y. Koval, P. Müller, R. Kleiner, D. A. Ryndyk, J. Keller, and C. Helm, Phys. Rev. B **67**, 024510 (2003).
[29] T. Koyama and M. Tachiki, Phys. Rev. B **54**, 16183 (1996).
[30] A. Irie and G. Oya, Supercond. Sci. Technol. **20**, S18 (2007).
[31] A. Irie and G. Oya, Physica C **293**, 249 (1997).
[32] C. S. Owen and D. J. Scalapino, Phys. Rev. Lett. **28**, 1559 (1972).
[33] W. H. Parker, Phys. Rev. B **12**, 3667 (1975).
[34] M. Tinkham, *Introduction to Superconductivity*, 2nd ed. (McGraw-Hill, New York, 1996).